Rectangular lattice Boltzmann method

Jian Guo Zhou
School of Engineering, University of Liverpool, Liverpool L69 3GQ, United Kingdom
(Received 10 September 2009; revised manuscript received 6 January 2010; published 16 February 2010)

A set of rectangular lattice Boltzmann methods for fluid flows is developed. It is shown that reformulating local equilibrium distribution functions can result in the rectangular lattice Boltzmann models without the aid of an interpolation for shallow water equations, Navier-Stokes equations, and axisymmetric flow equations. In addition, schemes for correct incorporation of force terms into the models are proposed for simulations of flows involving forces in practice. The methods completely retain the innate kinetic features and the simple procedure of the standard lattice Boltzmann method with an additional benefit of being suitable for rectangular lattices at little extra computational cost. The methodology is illustrated and validated through its application to different flow problems, demonstrating the potential power of the models.

DOI: 10.1103/PhysRevE.81.026705 PACS number(s): 47.11.−j

I. INTRODUCTION

The lattice Boltzmann method has been shown to be a successful computational method with a potential capability of simulating fluid flows in different areas [1–7]. The method is characterized by its simple procedure, easy treatment of boundary conditions and parallel feature in programming. This may make the method an efficient technique to model complicated physical phenomena in science and engineering.

Over the past years, the study on the lattice Boltzmann method has received increasing attention, greatly improving and developing the method. The main restriction of the method on a uniform square lattice has been investigated. Chew *et al.* [8], Mei and Shyy [9], and Stiebler *et al.* [10] transformed the lattice Boltzmann equation to its differential form so that they solved it with one of conventional numerical methods such as finite volume method on arbitrary meshes, showing the strength of the method. The drawback is that it loses the original simplicity of the lattice Boltzmann method and requires additional effort for mesh generation. Filippova and Hänel [11] proposed a simple scheme for patched grid refinement in the region around a solid body for the lattice Boltzmann method. However, the method involves more procedure to ensure correct transitions for physical variables such as pressure, velocity, and stresses at different mesh levels. Compared to above complex schemes, He *et al.* [12] formulated a relatively simple lattice Boltzmann model on a rectangular lattice by using an interpolation method, which retains most of the desirable features of the standard method on a square lattice. Subsequently, the similar procedure is applied to the lattice Boltzmann method for solving many different problems [13–15], indicating that a nonuniform lattice is desirable in practical applications. The primary downside is that the methods rely on interpolation schemes with complicated procedure, which introduce additional numerical viscosities and other artifacts into the lattice Boltzmann method as indicated by Lallemand and Luo [16]. To remove interpolations, Bouzidi *et al.* [17] proposed a lattice Boltzmann method on a two-dimensional (2D) rectangular grid with the multiple relaxation times (MRTs). The use of the MRT provides extra control of the model and successfully eliminates interpolations in the numerical procedure. The disadvantage is that the model still involves complicated procedure compared with the standard lattice Boltzmann method.

In this paper, an effort is made to formulate simple lattice Boltzmann methods for fluid flows on a rectangular lattice with the same desirable features as that of the standard lattice Boltzmann method on a square lattice. The methodology has been applied to developing rectangular lattice Boltzmann models for shallow water equations, Navier-Stokes equations, and axisymmetric flow equations in order to demonstrate its applicability and potential for fluid flows. The methods are automatically suitable for either square or rectangular lattices without a modification. Different numerical tests have been presented for the verification of the methods.

II. LATTICE BOLTZMANN METHOD

The following lattice Boltzmann equation is proposed for a model on either square or rectangular lattices:

$$f_\alpha(\mathbf{x}+\mathbf{e}_\alpha\Delta t,t+\Delta t)-f_\alpha(\mathbf{x},t)=-\frac{1}{\tau}(f_\alpha-f_\alpha^{eq})+\mathcal{Z}_\alpha\Delta t, \quad (1)$$

where τ is the single relaxation time [18], t is the time, f_α is the distribution function of particles, f_α^{eq} is the local equilibrium distribution function (EDF), Δt is the time step, $\mathbf{x}$ is the space vector defined by the Cartesian coordinate system, i.e., $\mathbf{x}=(x,y)$ in 2D space and $\mathbf{x}=(x,y,z)$ for three-dimensional (3D), $\mathcal{Z}_\alpha$ is related to a force term which is specified by Eq. (3), and $\mathbf{e}_\alpha$ is the particle velocity vector in the α link, which, e.g., for a 2D rectangular lattice with nine particle velocities (D2Q9) shown in Fig. 1, is defined as

$$\mathbf{e}_\alpha=\begin{cases}(0,0), & \alpha=0\\ (\pm e_x,0),(0,\pm e_y), & \alpha=1-4\\ (\pm e_x,\pm e_y), & \alpha=5-8,\end{cases} \quad (2)$$

in which $e_x=\Delta x/\Delta t$, $e_y=\Delta y/\Delta t$ with lattice sizes of Δx and Δy in x and y directions. It becomes a square lattice when $\Delta x=\Delta y$. For this rectangular lattice, $\mathcal{Z}_\alpha$ can generally be expressed by

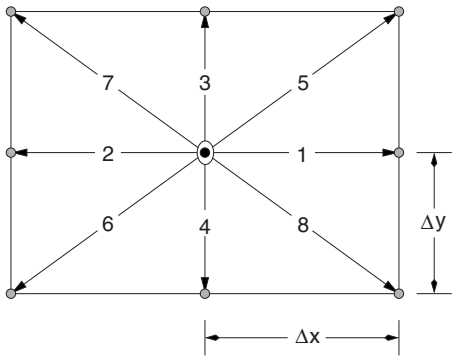

FIG. 1. Nine-velocity rectangular lattice (D2Q9).

$$\mathcal{Z}_\alpha = \begin{cases} 0, & \alpha = 0 \\ \dfrac{F_x}{6e_{\alpha x}}, & \alpha = 1 \text{ and } 2 \\ \dfrac{F_y}{6e_{\alpha y}}, & \alpha = 3 \text{ and } 4 \\ \dfrac{F_i}{6e_{\alpha i}}, & \alpha = 5-8. \end{cases} \tag{3}$$

In the above equation, F_i stands for all the force terms in the flow equations, whose detailed expression varies from one case to another and can be specified for a flow problem. It can be shown that $\mathcal{Z}_\alpha$ has the properties,

$$\sum_\alpha \mathcal{Z}_\alpha = 0, \quad \sum_\alpha e_{\alpha i}\mathcal{Z}_\alpha = F_i, \tag{4}$$

which are the necessary conditions for the conservation of mass and momentum in the lattice Boltzmann approach.

A. Shallow water equations

Shallow water equations are widely used as a mathematical model for a variety of fluid flows such as tidal flows, waves, open channel flows, dam breaks, and atmospheric flows. In the lattice Boltzmann theory, only if the local equilibrium distribution function is properly defined can the lattice Boltzmann Eq. (1) be employed to simulate certain flow equations [5]. For shallow water equations, the following expression is motivated (see Appendix A for detail):

$$f_\alpha^{eq} = \begin{cases} h - \sum_{\alpha=1}^{8} f_\alpha^{eq}, & \alpha = 0 \\ \left(\dfrac{gh}{4e_x^2} + \dfrac{u_x}{3e_{\alpha x}} + \dfrac{u_x^2}{2e_x^2}\right)h, & \alpha = 1 \text{ and } 2 \\ \left(\dfrac{gh}{4e_y^2} + \dfrac{u_y}{3e_{\alpha y}} + \dfrac{u_y^2}{2e_y^2}\right)h, & \alpha = 3 \text{ and } 4 \\ \left(\dfrac{u_i}{12e_{\alpha i}} + \dfrac{u_x u_y}{4e_{\alpha x}e_{\alpha y}}\right)h, & \alpha = 5-8. \end{cases} \tag{5}$$

The common force terms associated with shallow water flows are [5]

$$F_i = -gh\frac{\partial z_b}{\partial x_i} - \frac{\tau_{bi}}{\rho} + \frac{\tau_{wi}}{\rho} + E_i, \tag{6}$$

where x_i is the Cartesian coordinate, z_b is the bed elevation above datum, ρ is the water density, τ_{bi} is the bed shear stress in i direction defined by the velocities, τ_{wi} is the wind shear stress, and E_i is the Coriolis force.

The physical variables, water depth h, and flow velocity u_i are calculated from the distribution function,

$$h = \sum_\alpha f_\alpha, \quad u_i = \frac{1}{h}\sum_\alpha e_{\alpha i} f_\alpha. \tag{7}$$

Applying the Chapman-Enskog procedure can show that the lattice Boltzmann Eq. (1) recovers the shallow water equations,

$$\frac{\partial h}{\partial t} + \frac{\partial (hu_j)}{\partial x_j} = 0, \tag{8}$$

$$\frac{\partial (hu_i)}{\partial t} + \frac{\partial (hu_i u_j)}{\partial x_j} = F_i - \frac{g}{2}\frac{\partial h^2}{\partial x_i} + \nu\frac{\partial^2 (hu_i)}{\partial x_j^2}, \tag{9}$$

with the kinematic viscosity ν,

$$\nu = \frac{e_x e_y \Delta t}{6}(2\tau - 1). \tag{10}$$

B. Navier-Stokes equations

The Navier-Stokes equations together with the continuity equation are the general governing equations for fluid flows. In order to formulate a rectangular lattice Boltzmann model for the equations, we propose the following local equilibrium distribution function for the 2D nine-velocity rectangular lattice (see Fig. 1),

$$f_\alpha^{eq} = \begin{cases} \rho - \sum_{\alpha=1}^{8} f_\alpha^{eq}, & \alpha = 0 \\ \left(\omega\dfrac{e_y}{e_x} + \dfrac{u_x}{3e_{\alpha x}} + \dfrac{u_x^2}{2e_x^2}\right)\rho, & \alpha = 1 \text{ and } 2 \\ \left(\omega\dfrac{e_x}{e_y} + \dfrac{u_y}{3e_{\alpha y}} + \dfrac{u_y^2}{2e_y^2}\right)\rho, & \alpha = 3 \text{ and } 4 \\ \left(\dfrac{u_i}{12e_{\alpha i}} + \dfrac{u_x u_y}{4e_{\alpha x}e_{\alpha y}}\right)\rho, & \alpha = 5-8, \end{cases} \tag{11}$$

in which ω is a free constant and its value may affect stability. As an individual modulus of each distribution function must be less than the sum of all the distribution functions regardless of velocities, it follows that

$$\omega\frac{e_y}{e_x} < 1, \quad \omega\frac{e_x}{e_y} < 1, \tag{12}$$

from which, we obtain

$$\omega < \min\left\{\frac{e_x}{e_y}, \frac{e_y}{e_x}\right\} \le 1 \tag{13}$$

or

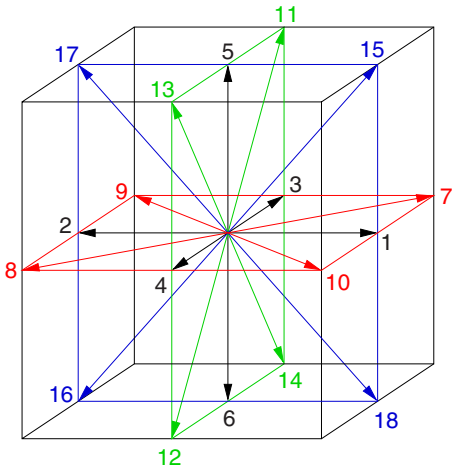

FIG. 2. (Color online) Nineteen-velocity cuboid lattice (D3Q19).

$$\omega < \min\left\{\frac{\Delta x}{\Delta y}, \frac{\Delta y}{\Delta x}\right\} \leq 1. \tag{14}$$

If a lattice ratio is defined as

$$\gamma = \min\left\{\frac{\Delta x}{\Delta y}, \frac{\Delta y}{\Delta x}\right\} = \min\left\{\frac{e_x}{e_y}, \frac{e_y}{e_x}\right\}, \tag{15}$$

then $\omega < \gamma \leq 1$. This suggests that smaller ω should be used for small lattice ratio γ, which may affect the accuracy like other numerical methods. However, numerical calculations indicate that the method is stable and accurate with a value of $\omega \leq 1/6$, which can produce an ω-independent accurate solution. It is also apparent that $\gamma < 1$ means a rectangular lattice and $\gamma = 1$ means a square lattice.

For a model on a 3D nineteen-velocity cuboid lattice (D3Q19) shown in Fig. 2, the following local equilibrium distribution function will be used:

$$f_\alpha^{eq} = \begin{cases} \rho - \sum_{\alpha=1}^{18} f_\alpha^{eq}, & \alpha = 0 \\ \left(\omega \frac{e_y e_z}{e_x e} + \frac{u_x}{3e_{\alpha x}} + \frac{u_x^2}{2e_x^2}\right)\rho, & \alpha = 1 \text{ and } 2 \\ \left(\omega \frac{e_x e_z}{e_y e} + \frac{u_y}{3e_{\alpha y}} + \frac{u_y^2}{2e_y^2}\right)\rho, & \alpha = 3 \text{ and } 4 \\ \left(\omega \frac{e_x e_y}{e_z e} + \frac{u_z}{3e_{\alpha z}} + \frac{u_z^2}{2e_z^2}\right)\rho, & \alpha = 5 \text{ and } 6 \\ \left(\frac{u_x}{24e_{\alpha x}} + \frac{u_y}{24e_{\alpha y}} + \frac{u_x u_y}{4e_{\alpha x} e_{\alpha y}}\right)\rho, & \alpha = 7 - 10 \\ \left(\frac{u_y}{24e_{\alpha y}} + \frac{u_z}{24e_{\alpha z}} + \frac{u_y u_z}{4e_{\alpha y} e_{\alpha z}}\right)\rho, & \alpha = 11 - 14 \\ \left(\frac{u_x}{24e_{\alpha x}} + \frac{u_z}{24e_{\alpha z}} + \frac{u_x u_z}{4e_{\alpha x} e_{\alpha z}}\right)\rho, & \alpha = 15 - 18, \end{cases} \tag{16}$$

where

$$e_z = \frac{\Delta z}{\Delta t}, \quad e = \frac{\Delta x + \Delta y + \Delta z}{3\Delta t}, \tag{17}$$

in which Δz is the lattice size in the vertical direction and the particle velocity vector for D3Q19 is

$$\mathbf{e}_\alpha = \begin{cases} (0,0,0), & \alpha = 0 \\ (\pm e_x,0,0),(0,\pm e_y,0),(0,0,\pm e_z), & \alpha = 1 - 6 \\ (\pm e_x, \pm e_y, 0), & \alpha = 7 - 10 \\ (0, \pm e_y, \pm e_z), & \alpha = 11 - 14 \\ (\pm e_x, 0, \pm e_z), & \alpha = 15 - 18. \end{cases} \tag{18}$$

Accordingly, Eq. (3) for $\mathcal{Z}_\alpha$ needs to be replaced by

$$\mathcal{Z}_\alpha = \begin{cases} 0, & \alpha = 0 \\ \frac{F_x}{10e_{\alpha x}}, & \alpha = 1 \text{ and } 2 \\ \frac{F_y}{10e_{\alpha y}}, & \alpha = 3 \text{ and } 4 \\ \frac{F_z}{10e_{\alpha z}}, & \alpha = 5 \text{ and } 6 \\ \frac{F_x}{10e_{\alpha x}} + \frac{F_y}{10e_{\alpha y}}, & \alpha = 7 - 10 \\ \frac{F_y}{10e_{\alpha y}} + \frac{F_z}{10e_{\alpha z}}, & \alpha = 11 - 14 \\ \frac{F_x}{10e_{\alpha x}} + \frac{F_z}{10e_{\alpha z}}, & \alpha = 15 - 18, \end{cases} \tag{19}$$

which also holds the properties specified by Eq. (4).

The detail of using the Chapman-Enskog procedure for recovery of the following incompressible Navier-Stokes equations is given in Appendix B:

$$\frac{\partial u_j}{\partial x_j} = 0, \tag{20}$$

$$\frac{\partial u_i}{\partial t} + \frac{\partial (u_i u_j)}{\partial x_j} = \frac{F_i}{\rho} - \frac{1}{\rho}\frac{\partial p}{\partial x_i} + \nu \frac{\partial^2 u_i}{\partial x_j^2}, \tag{21}$$

in which the kinematic viscosity ν is given by Eq. (10) for 2D case and for 3D it can be calculated as

$$\nu = \frac{e_x e_y e_z \Delta t}{6e}(2\tau - 1), \tag{22}$$

which differs from that for the standard lattice Boltzmann method on a square lattice and reflects the effect of a rectangular lattice, which is similar to that pointed out by Bouzidi *et al.* [17] in their MRT model on a rectangular lattice. When $\gamma = 1$ or a square lattice is applied, the kinematic viscosity ν given by either Eq. (10) or Eq. (22) reverts to that for the conventional lattice Boltzmann method; also the same sound speed of $e/\sqrt{3}$ is recovered if $\omega = 1/6$ is used, in which $e = e_x = e_y$. This is also consistent with the reported studies by Bouzidi *et al.* [17].

The density ρ and flow velocity u_i are determined from the distribution function,

$$\rho = \sum_\alpha f_\alpha, \quad u_i = \frac{1}{\rho}\sum_\alpha e_{\alpha i} f_\alpha. \tag{23}$$

C. Axisymmetric flow equations

Axisymmetric flows represent numerous important flow problems in practice [19–23]. In theory, 3D axisymmetric flows are effectively 2D problems in a cylindrical coordinate system. To make use of this advantage, Halliday *et al.* [24] first studied the lattice Boltzmann method for axisymmetric flows in 2001. Since then, a few more methods have been developed [22,25,26]. Here, we take Zhou's model [25] as an example to formulate a rectangular lattice Boltzmann model on D2Q9 (see Fig. 1) and the methodology can be extended to the other schemes such as the method of Guo *et al.* [26]. In Zhou's model, the lattice Boltzmann Eq. (1) includes an additional source or sink term θ,

$$f_\alpha(\mathbf{x}+\mathbf{e}_\alpha\Delta t, t+\Delta t) - f_\alpha(\mathbf{x},t) = -\frac{1}{\tau}(f_\alpha - f_\alpha^{eq}) + \theta\Delta t + \mathcal{Z}_\alpha\Delta t. \tag{24}$$

Since a 3D axisymmetric flow is a 2D flow problem, the local equilibrium distribution function (11) and the expression (3) for $\mathcal{Z}_\alpha$ can directly be used. Again, employing the Chapman-Enskog analysis shows that the lattice Boltzmann Eq. (24) can simulate the following axisymmetric flow equations in a 2D cylindrical coordinate system (x,r),

$$\frac{\partial u_j}{\partial x_j} = -\frac{u_r}{r}, \tag{25}$$

$$\frac{\partial u_i}{\partial t} + \frac{\partial (u_i u_j)}{\partial x_j} = -\frac{1}{\rho}\frac{\partial p}{\partial x_i} + \nu\frac{\partial^2 u_i}{\partial x_j^2} + \frac{F_i}{\rho}, \tag{26}$$

in which

$$\theta = -\frac{\rho}{9}\frac{u_r}{r} \tag{27}$$

and

$$F_i = \rho\left(\frac{\nu}{r}\frac{\partial u_i}{\partial r} - \frac{u_i u_r}{r} - \frac{\nu u_i}{r^2}\delta_{ir}\right), \tag{28}$$

where x and r are the coordinates in axial and radial directions, respectively, and δ_{mn} is the Kronecker delta function defined by

$$\delta_{mn} = \begin{cases} 0, & m \neq n \\ 1, & m = n. \end{cases} \tag{29}$$

Similarly, Eq. (23) is used to calculate the density ρ and flow velocity u_i.

III. NUMERICAL EXAMPLES

The proposed methods are applied to solving different flow problems. They cover typical shallow water flow problems (a still flow over a bump, a tidal flow over an irregular bed topography, a flow in a straight channel, and a flow through a strongly curved bend channel), 2D Couette-Poiseuille flow, and 3D Womersley flow. In the simulations, the bounce-back scheme is applied to no-slip boundary condition and the elastic-collision scheme [27] is applied to semislip or slip boundary conditions. All the dimensional physical variables in SI units are used.

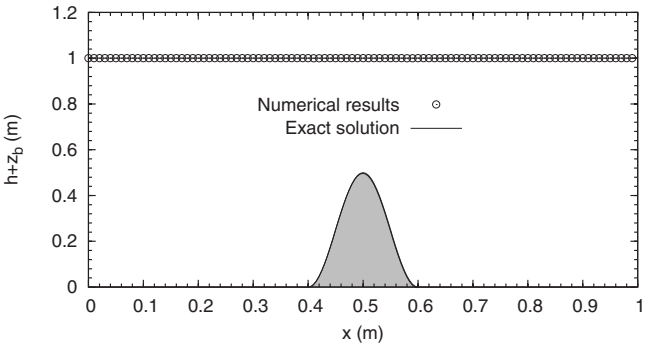

FIG. 3. Comparison of profile with exact solution.

A. Stationary case

The first problem is a still flow over a bump in a channel. This is a benchmark test to validate a numerical method for shallow water flows. As there is a nonzero force associated with the bed slope in the shallow water equations in this case, many numerical methods fail to reproduce the exact solution; hence it is an appropriate case to verify the treatment of the force term in the proposed methods. The bed topography is the same as that used by LeVeque [28] and is given by

$$z_b(x) = \begin{cases} 0.25\left[\cos\dfrac{\pi(x-0.5)}{0.1} + 1\right], & |x-0.5| < 0.1 \\ 0, & \text{otherwise}. \end{cases} \tag{30}$$

The channel has the length of 1. In the numerical computations, the 2D code is purposely applied with 200×25 rectangular lattices: $\Delta y = 0.0025$, $\Delta x = 2\Delta y$, $\Delta t = 0.0001$, and $\tau = 1.2$. The initial conditions are $u_i = 0$ and $h + z_b = 1$, for which the exact solution is also $u_i \equiv 0$ and $h + z_b \equiv 1$. After a steady solution is reached, it is found that the numerical results are accurate up to computer precision and the comparisons for water level and velocity are plotted in Figs. 3 and 4, respectively, confirming the accuracy of the proposed method.

B. Tidal flow

The second is a tidal flow over an irregular bed as a further test, which is a common flow problem in coastal engineering. The bed is defined with the data listed in Table I. The initial and boundary conditions are

$$h(x,0) = 16 - z_b(x), \tag{31}$$

$$u_x(x,0) = 0 \tag{32}$$

and

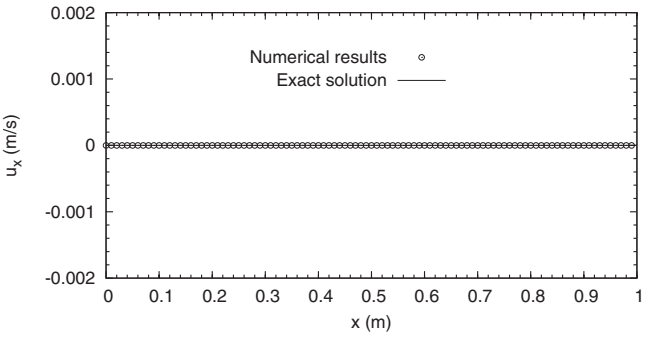

FIG. 4. Comparison of velocity with exact solution.

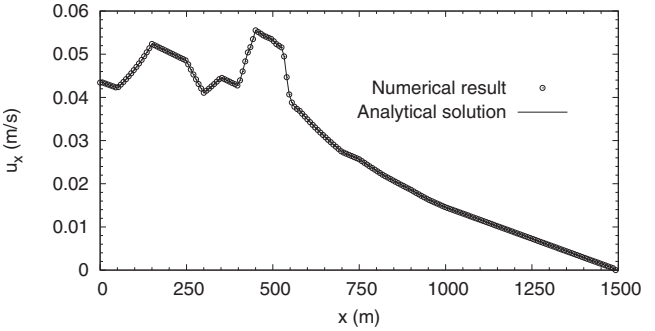

FIG. 5. Comparison of velocity at $t=10\,800$ s.

$$h(0,t) = 20 - 4\,\sin\left[\pi\left(\frac{4t}{86\,400} + \frac{1}{2}\right)\right], \tag{33}$$

$$u_x(L,t) = 0, \tag{34}$$

where $L=1500$ is the channel length.

Under these conditions, the tidal flow is relatively short and an asymptotic analytical solution is [29]

$$h(x,t) = 20 - z_b(x) - 4\,\sin\left[\pi\left(\frac{4t}{86\,400} + \frac{1}{2}\right)\right] \tag{35}$$

and

$$u_x(x,t) = \frac{(x-L)\pi}{5400h(x,t)}\cos\left[\pi\left(\frac{4t}{86\,400} + \frac{1}{2}\right)\right]. \tag{36}$$

In the simulation, rectangular lattices with 200×25 cells are also used: $\Delta x=7.5$, $\Delta y=2\Delta x$, $\Delta t=0.3$, and $\tau=1.5$. In order to compare the numerical results with the asymptotic analytical solution, we choose two numerical results at $t=10\,800$ and $t=32\,400$, which correspond to the half-risen tidal flow with maximum positive velocities and to the half-ebb tidal flow with maximum negative velocities. Comparisons of velocities are depicted in Figs. 5 and 6, respectively. This shows excellent agreements between the numerical predictions and the analytical solutions.

C. 2D flow in a straight channel

The third test is a steady flow through a straight channel with the width of $2y_0=0.8$. The analytical solution is a parabolic profile for the velocity component u_x in the streamline direction,

$$u_x(y) = U_0\left[1 - \left(\frac{y-y_0}{y_0}\right)^2\right]. \tag{37}$$

The discharge $Q=0.0123$ is specified at the inflow boundary. 200×40 rectangular lattices are used with $\Delta y=0.02$, $\Delta x=2\Delta y$, $\Delta t=0.004$, and $\tau=0.7$. After the steady solution is obtained, the velocity profile is shown in Fig. 7 and compared with the analytical solution in the figure, revealing excellent agreement.

D. Flow in a strongly curved bend channel

The forth is a steady flow through a strongly curved bend channel, which represents one of the most complex flows encountered in a natural meandering river. The same flow in a 180° bend channel as Run No. 8 of Rozovskii's experiments [30] shown in Fig. 8 is simulated. The channel width is 0.8; the internal radius is 0.4; and there is no bed slope. The flow conditions are: flow discharge is 0.0123; entrance water depth is 0.063; and the channel bed is rough with Chezy coefficient $C_z=32$.

In numerical computation, 400×125 square lattices are used. $\Delta x=\Delta y=0.02$, $\Delta t=0.013\,33$, and $\tau=0.6$. At the upstream boundary, velocity u_x is adjusted to retain the constant discharge; and $u_y=0$. At the downstream boundary the depth is specified as 0.05. These conditions are transformed to suitable conditions for distribution functions with the method described by Zhou [5]. At the channel sides, the semislip boundary conditions are used with $C_f=0.03$ [5].

A steady solution is achieved after 5000 iterations. Comparisons of the tangential velocities between numerical results and experimental data at several cross sections are depicted in Fig. 8, showing good agreements. In addition, the numerical results are also obtained with the lattice Boltzmann method for shallow water flows (LABSWE) using the

TABLE I. Bed elevation z_b for irregular bed.

$x(m)$	0	50	100	150	250	300	350	400	425	435
$z_b(m)$	0	0	2.5	5	5	3	5	5	7.5	8
$x(m)$	450	475	500	505	530	550	565	575	600	650
$z_b(m)$	9	9	9.1	9	9	6	5.5	5.5	5	4
$x(m)$	700	750	800	820	900	950	1000	1500		
$z_b(m)$	3	3	2.3	2	1.2	0.4	0	0		

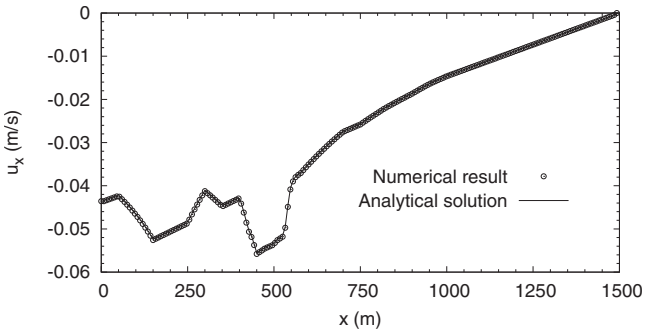

FIG. 6. Comparison of velocity at $t=32\,400$ s.

original local equilibrium distribution function [31] and are shown in the figure, which indicates that both results are almost identical. This further confirms the accuracy of the proposed method.

E. Couette-Poiseuille flow

The fifth is a numerical simulation of the Couette-Poiseuille flow to verify the rectangular lattice Boltzmann model for Navier-Stokes equations. This is a steady flow within parallel plane boundaries and driven by constant pressure gradient with the following analytical solution [32]:

$$u_x(y) = U_t\frac{y}{2y_0} + U_0\left[1 - \left(\frac{y-y_0}{y_0}\right)^2\right], \tag{38}$$

where U_t is the velocity component u_x of the plane at $y=2y_0$ in the x direction. The boundary conditions are

$$u_x(y) = \begin{cases} 0, & y = 0 \\ U_t, & y = 2y_0 \end{cases} \tag{39}$$

and

$$u_y(y) = 0. \tag{40}$$

We consider here three different cases with $U_t=0$, $U_t=0.1$, and $U_t=-0.1$ for a discharge $Q=0.3$. The width between the two planes is $2y_0=1.5$ and the length is 4.95. At the inflow boundary, the discharge is specified. At the plane boundaries,

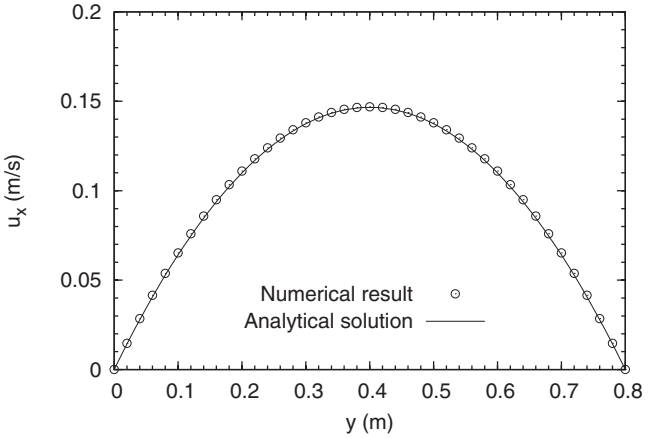

FIG. 7. Comparison of velocity profile.

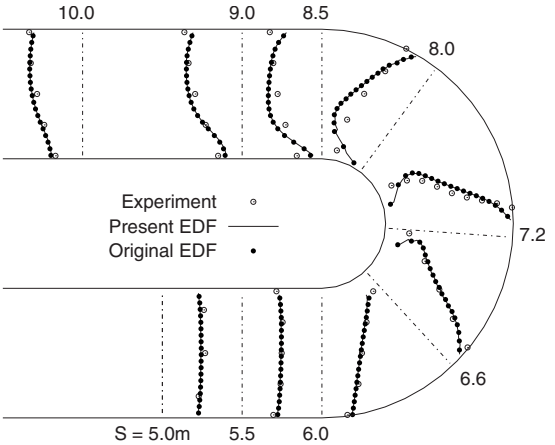

FIG. 8. Comparisons of the tangential velocities (S is distance between cross section and entrance along channel central line).

for $y=0$, no-slip boundary condition is applied, and for $y=2y_0$, the unknown distribution functions f_4, f_6, f_8, and ρ can be determined following the scheme by Zou and He [33] based on the boundary conditions (39) and (40) as

$$\rho = [f_0 + f_1 + f_2 + 2(f_3 + f_5 + f_7)], \tag{41}$$

$$f_4 = f_3, \tag{42}$$

$$f_6 = f_5 + \frac{1}{2}(f_1 - f_2) - \frac{\rho U_t}{2e_x}, \tag{43}$$

$$f_8 = f_7 - \frac{1}{2}(f_1 - f_2) + \frac{\rho U_t}{2e_x}. \tag{44}$$

66×40 rectangular lattices are used with $\Delta y=0.0375$, $\Delta x=2\Delta y$, $\Delta t=0.0375$, $\tau=0.7$, and $\rho=1000$ in all the computations. After the steady solutions are reached, we compare the numerical results with the analytical solutions, which are plotted in Fig. 9, showing excellent agreements.

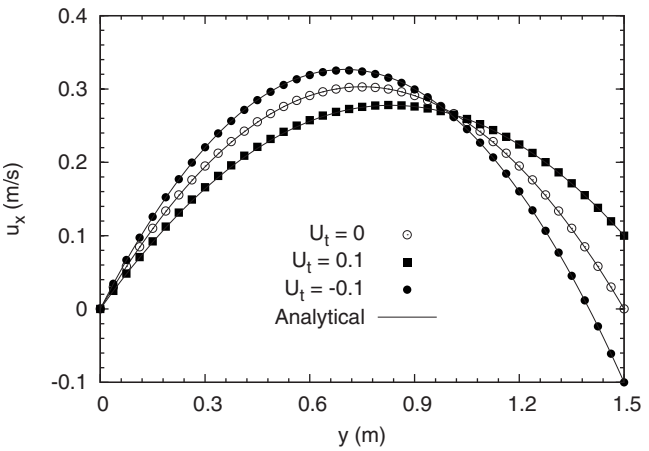

FIG. 9. Comparisons of velocity profiles (symbols stand for numerical results).

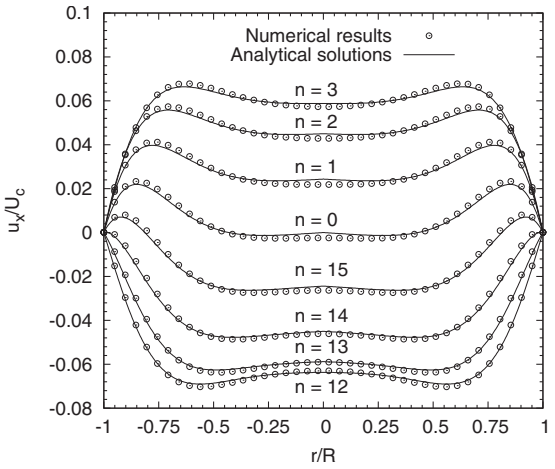

FIG. 10. Comparisons when u_x is increasing at different time $t=nT/16$ with $n=0,1,2,3,12,13,14,15$.

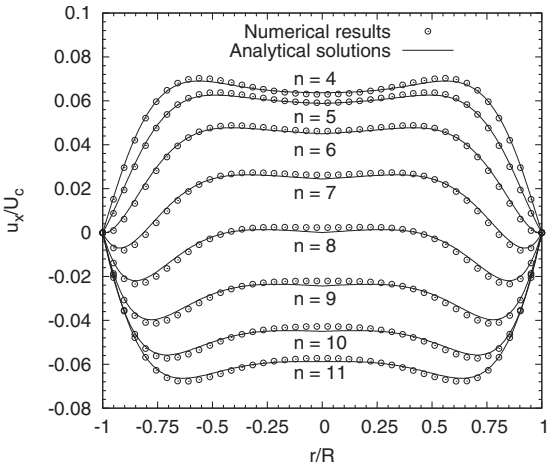

FIG. 11. Comparisons when u_x is decreasing at different time $t=nT/16$ with $n=4,5,6,7,8,9,10,11$.

F. 3D Womersley flow

The last is the prediction of a 3D Womersley flow or a pulsatile flow in a pipe to validate the rectangular lattice Boltzmann model for axisymmetric flow. The flow is driven by a periodic pressure gradient at the inlet of the pipe and the pressure gradient is normally given by

$$\frac{dp}{dx} = p_0 \cos(\Omega t), \tag{45}$$

where p_0 is the maximum amplitude of the pressure variation and $\Omega=2\pi/T$ is the angular frequency, in which T is the period.

The Reynolds number is defined as $R_e=U_cD/\nu$ with the characteristic velocity U_c given by

$$U_c = \frac{p_0\beta^2}{4\Omega\rho} = \frac{p_0R^2}{4\rho\nu}, \tag{46}$$

in which $\beta=R\sqrt{\Omega/\nu}$ is the Womersley number, where R is the pipe radius and D is the diameter. The analytical solution for the velocity component in axial direction for the Womersley flow is

$$u_x(r,t) = \mathrm{Re}\left\{\frac{p_0}{i\Omega\rho}\left[1 - \frac{J_0(r\phi/R)}{J_0(\phi)}\right]e^{i\Omega t}\right\}, \tag{47}$$

where J_0 is the zeroth order Bessel function of the first type, i is the imaginary unit, $\phi=(-\beta+i\beta)/\sqrt{2}$, and Re denotes the real part of a complex number.

In the computation, $\rho=3$, $p_0=0.001$, $D=40$, $T=1200$, $\beta=8$, and $U_C=1$, which give $R_e=1200$. 80×42 rectangular lattices with $\Delta y=0.97561$ and $\Delta x=1.5\Delta y$ as well as $\Delta t=0.9518$ and $\tau=0.6$ are used in the simulation. The numerical solutions at different times are obtained after initial running time of $10T$. The corresponding results for velocity u_x are shown in Figs. 10 and 11, in which they are further compared with the analytical solution (47), exhibiting good agreements.

IV. CONCLUSIONS

Rectangular lattice Boltzmann methods for fluid flows are presented. Numerical verifications have been carried out by simulations of different shallow water flows, Couette-Poiseuille flow and Womersley flow, showing good agreements between the numerical results and analytical solutions. The models are simple and accurate at the same simple procedure on either square or rectangular lattices as that of the standard lattice Boltzmann method at little additional computational cost. This provides further flexibility for solving flow problems. The methodology can be extended to the lattice Boltzmann method for other flow equations, leading to a wide range of applications in science and engineering.

ACKNOWLEDGMENT

The author is grateful to the referee's useful comments and suggestions.

APPENDIX A: MOTIVATION FOR THE LOCAL EQUILIBRIUM DISTRIBUTION FUNCTION

According to the lattice Boltzmann approaches, the correct recovery of the macroscopic equations requires that the local equilibrium distribution functions must satisfy

$$\sum_\alpha f_\alpha^{eq} = h, \tag{A1}$$

$$\sum_\alpha e_{\alpha i} f_\alpha^{eq} = hu_i, \tag{A2}$$

$$\sum_\alpha e_{\alpha i} e_{\alpha j} f_\alpha^{eq} = \frac{1}{2} g h^2 \delta_{ij} + hu_i u_j, \tag{A3}$$

for the shallow water equations and

$$\sum_\alpha f_\alpha^{eq} = \rho, \tag{A4}$$

$$\sum_{\alpha} e_{\alpha i} f_{\alpha}^{eq} = \rho u_i, \tag{A5}$$

$$\sum_{\alpha} e_{\alpha i} e_{\alpha j} f_{\alpha}^{eq} = p\delta_{ij} + \rho u_i u_j, \tag{A6}$$

for the Navier-Stokes equations.

Taking account of the symmetric features of the rectangular lattice, we may suggest that the local equilibrium distribution function, e.g., for D2Q9, has the following form:

$$f_{\alpha}^{eq} = \begin{cases} \left(A_0 + A_1 \dfrac{u_x}{e_{\alpha x}} + A_2 \dfrac{u_x^2}{e_x^2}\right)\lambda, & \alpha = 1 \text{ and } 2 \\ \left(B_0 + B_1 \dfrac{u_y}{e_{\alpha y}} + B_2 \dfrac{u_y^2}{e_y^2}\right)\lambda, & \alpha = 3 \text{ and } 4 \\ \left(C_1 \dfrac{u_i}{e_{\alpha i}} + C_2 \dfrac{u_x u_y}{e_{\alpha x} e_{\alpha y}}\right)\lambda, & \alpha = 5 - 8 \end{cases} \tag{A7}$$

and

$$f_0^{eq} = \lambda - \sum_{\alpha=1}^{8} f_{\alpha}^{eq}, \tag{A8}$$

in which $\lambda = h$ for the shallow water equations or $\lambda = \rho$ for the Navier-Stokes equations.

Based on the aforementioned three constraints, after some mathematical manipulation, the coefficients in the above expression can be decided, leading to the local equilibrium distribution functions for the shallow water equations, Eq. (5), and for the Navier-Stokes equations, Eq. (11). Similarly, we can determine the expression for the local equilibrium distribution function (16) for 3D Navier-Stokes equations based on D3Q19.

It may be pointed out that, e.g., for the Navier-Stokes equations, combing constraints (A4) and (A5) with corresponding expression (23) for physical variables forms the conservation conditions for mass and momentum in the method [5],

$$\sum_{\alpha} f_{\alpha} = \sum_{\alpha} f_{\alpha}^{eq} \tag{A9}$$

and

$$\sum_{\alpha} e_{\alpha i} f_{\alpha} = \sum_{\alpha} e_{\alpha i} f_{\alpha}^{eq}. \tag{A10}$$

APPENDIX B: RECOVERY OF THE NAVIER-STOKES EQUATIONS

Without loss of generality, we apply the Chapman-Enskog analysis to recovering the 2D Navier-Stokes equations in detail and the similar procedure can be applied to recovery of the other flow equations like the shallow water equations.

Assuming Δt is small and

$$\Delta t = \varepsilon, \tag{B1}$$

substitution of Eq. (B1) into Eq. (1) leads to

$$f_{\alpha}(\mathbf{x} + \mathbf{e}_{\alpha}\varepsilon, t + \varepsilon) - f_{\alpha}(\mathbf{x}, t) = -\frac{1}{\tau}(f_{\alpha} - f_{\alpha}^{eq}) + \mathcal{Z}_{\alpha}\varepsilon. \tag{B2}$$

Taking a Taylor expansion to the left-hand side of the above equation in time and space around point $(\mathbf{x}, t)$, we have

$$\varepsilon\left(\frac{\partial}{\partial t} + e_{\alpha j}\frac{\partial}{\partial x_j}\right) f_{\alpha} + \frac{1}{2}\varepsilon^2\left(\frac{\partial}{\partial t} + e_{\alpha j}\frac{\partial}{\partial x_j}\right)^2 f_{\alpha} + \mathcal{O}(\varepsilon^3) = -\frac{1}{\tau}(f_{\alpha} - f_{\alpha}^{eq}) + \mathcal{Z}_{\alpha}\varepsilon. \tag{B3}$$

According to the Chapman-Enskog expansion, f_{α} can be written in a series of ε,

$$f_{\alpha} = f_{\alpha}^{(0)} + \varepsilon f_{\alpha}^{(1)} + \varepsilon^2 f_{\alpha}^{(2)} + \mathcal{O}(\varepsilon^3). \tag{B4}$$

The centered scheme [5] is used for the term $\mathcal{Z}_{\alpha}$,

$$\mathcal{Z}_{\alpha} = \mathcal{Z}_{\alpha}\left(\mathbf{x} + \frac{1}{2}\mathbf{e}_{\alpha}\varepsilon, t + \frac{1}{2}\varepsilon\right), \tag{B5}$$

which can also be written, via a Taylor expansion, as

$$\mathcal{Z}_{\alpha}\left(\mathbf{x} + \frac{1}{2}\mathbf{e}_{\alpha}\varepsilon, t + \frac{1}{2}\varepsilon\right) = \mathcal{Z}_{\alpha} + \frac{1}{2}\varepsilon\left(\frac{\partial}{\partial t} + e_{\alpha j}\frac{\partial}{\partial x_j}\right)\mathcal{Z}_{\alpha} + \mathcal{O}(\varepsilon^2). \tag{B6}$$

After inserting Eqs. (B4) and (B6) into Eq. (B3), the equation to order ε^0 is

$$f_{\alpha}^{(0)} = f_{\alpha}^{eq} \tag{B7}$$

to order ε

$$\left(\frac{\partial}{\partial t} + e_{\alpha j}\frac{\partial}{\partial x_j}\right) f_{\alpha}^{(0)} = -\frac{1}{\tau} f_{\alpha}^{(1)} + \mathcal{Z}_{\alpha} \tag{B8}$$

and to order ε^2

$$\left(\frac{\partial}{\partial t} + e_{\alpha j}\frac{\partial}{\partial x_j}\right) f_{\alpha}^{(1)} + \frac{1}{2}\left(\frac{\partial}{\partial t} + e_{\alpha j}\frac{\partial}{\partial x_j}\right)^2 f_{\alpha}^{(0)} = -\frac{1}{\tau} f_{\alpha}^{(2)} + \frac{1}{2}\left(\frac{\partial}{\partial t} + e_{\alpha j}\frac{\partial}{\partial x_j}\right)\mathcal{Z}_{\alpha}. \tag{B9}$$

Applying Eq. (B8), we can write the above equation as

$$\left(1 - \frac{1}{2\tau}\right)\left(\frac{\partial}{\partial t} + e_{\alpha j}\frac{\partial}{\partial x_j}\right) f_{\alpha}^{(1)} = -\frac{1}{\tau} f_{\alpha}^{(2)}. \tag{B10}$$

From Eq. (B8) $+ \varepsilon \times$ Eq. (B10), we have

$$\left(\frac{\partial}{\partial t} + e_{\alpha j}\frac{\partial}{\partial x_j}\right) f_{\alpha}^{(0)} + \varepsilon\left(1 - \frac{1}{2\tau}\right)\left(\frac{\partial}{\partial t} + e_{\alpha j}\frac{\partial}{\partial x_j}\right) f_{\alpha}^{(1)} = -\frac{1}{\tau}(f_{\alpha}^{(1)} + \varepsilon f_{\alpha}^{(2)}) + \mathcal{Z}_{\alpha}. \tag{B11}$$

Summation of the above equation over α provides

$$\frac{\partial}{\partial t}\sum_{\alpha} f_{\alpha}^{(0)} + \frac{\partial}{\partial x_j}\sum_{\alpha} e_{\alpha j} f_{\alpha}^{(0)} = 0. \tag{B12}$$

Using the local equilibrium distribution function (11) to evaluate the terms in the above results in

$$\frac{\partial \rho}{\partial t} + \frac{\partial (\rho u_j)}{\partial x_j} = 0. \tag{B13}$$

If the density variation is small enough and can be neglected, the above becomes the continuity Eq. (20) for incompressible flows.

Taking $\Sigma e_{\alpha i}$[Eq. (B8)$+\varepsilon \times$Eq. (B10)] about α yields

$$\frac{\partial}{\partial t}\sum_{\alpha} e_{\alpha i} f_{\alpha}^{(0)} + \frac{\partial \Pi_{ij}^{(0)}}{\partial x_j} = \frac{\partial \Pi_{ij}^{(1)}}{\partial x_j} + F_i, \tag{B14}$$

where $\Pi_{ij}^{(0)}$ is the zeroth-order momentum flux tensor,

$$\Pi_{ij}^{(0)} = \sum_{\alpha} e_{\alpha i} e_{\alpha j} f_{\alpha}^{(0)}, \tag{B15}$$

and $\Pi_{ij}^{(1)}$ is the first-order momentum flux tensor,

$$\Pi_{ij}^{(1)} = -\frac{\varepsilon}{2\tau}(2\tau - 1)\sum_{\alpha} e_{\alpha i} e_{\alpha j} f_{\alpha}^{(1)}. \tag{B16}$$

Evaluating terms in Eq. (B15) with Eq. (11), we have

$$\Pi_{ij}^{(0)} = p\delta_{ij} + \rho u_i u_j, \tag{B17}$$

where $p = 2\rho\omega e_x e_y$ is the pressure, leading to a sound speed, $C_s = \sqrt{2\omega e_x e_y}$. Substitution of the above equation into Eq. (B14) results in

$$\frac{\partial (\rho u_i)}{\partial t} + \frac{\partial (\rho u_i u_j)}{\partial x_j} = F_i - \frac{\partial p}{\partial x_i} + \frac{\partial \Pi_{ij}^{(1)}}{\partial x_j}. \tag{B18}$$

Applying Eq. (B8) we can rewrite Eq. (B16) as

$$\Pi_{ij}^{(1)} = \frac{\varepsilon}{2}(2\tau - 1)\sum_{\alpha} e_{\alpha i} e_{\alpha j}\left(\frac{\partial}{\partial t} + e_{\alpha k}\frac{\partial}{\partial x_k}\right) f_{\alpha}^{(0)}, \tag{B19}$$

which can also be written with Eq. (B15) as

$$\Pi_{ij}^{(1)} = \frac{\varepsilon}{2}(2\tau - 1)\frac{\partial}{\partial t}\Pi_{ij}^{(0)} + \frac{\varepsilon}{2}(2\tau - 1)\frac{\partial}{\partial x_k}\sum_{\alpha} e_{\alpha i} e_{\alpha j} e_{\alpha k} f_{\alpha}^{(0)}. \tag{B20}$$

The second term in the above equation can be approximately evaluated with Eqs. (11) and (B7) as

$$\frac{\partial}{\partial x_k}\sum_{\alpha} e_{\alpha i} e_{\alpha j} e_{\alpha k} f_{\alpha}^{(0)} \approx \frac{e_x e_y}{3}\frac{\partial}{\partial x_k}(\rho u_i \delta_{jk} + \rho u_j \delta_{ki} + \rho u_k \delta_{ij}). \tag{B21}$$

If we assume that characteristic velocity is U_c, length L_c, and time t_c, we have that the term $(\partial/\partial t \Pi_{ij}^{(0)})$ is of order $\rho U_c^2/t_c$ and the term $(\partial/\partial x_k \Sigma_{\alpha} e_{\alpha i} e_{\alpha j} e_{\alpha k} f_{\alpha}^{(0)})$ is of order $\rho e_x e_y U_c/L_c$, based on which we obtain that the ratio of the former to the latter terms has the order,

$$\mathcal{O}\left(\frac{\partial/\partial t \Pi_{ij}^{(0)}}{\partial/\partial x_k \Sigma_{\alpha} e_{\alpha i} e_{\alpha j} e_{\alpha k} f_{\alpha}^{(0)}}\right) = \mathcal{O}\left(\frac{\rho U_c^2/t_c}{\rho e_x e_y U_c/L_c}\right) = \mathcal{O}\left(\frac{U_c}{\sqrt{e_x e_y}}\right)^2 = \mathcal{O}\left(\frac{U_c}{C_s}\right)^2 = \mathcal{O}(M^2), \tag{B22}$$

in which $M = U_c/C_s$ is the Mach number. It follows that the first term in Eq. (B20) is very small compared with the second term and can be neglected if $M \ll 1$; hence Eq. (B20) after Eq. (B21) is substituted becomes

$$\Pi_{ij}^{(1)} = \frac{e_x e_y \varepsilon}{6}(2\tau - 1)\frac{\partial}{\partial x_k}(\rho u_i \delta_{jk} + \rho u_j \delta_{ki} + \rho u_k \delta_{ij}) \tag{B23}$$

or

$$\Pi_{ij}^{(1)} = \nu\left[\frac{\partial (\rho u_i)}{\partial x_j} + \frac{\partial (\rho u_j)}{\partial x_i} + \frac{\partial (\rho u_k)}{\partial x_k}\delta_{ij}\right] \tag{B24}$$

with the kinematic viscosity defined by

$$\nu = \frac{e_x e_y \Delta t}{6}(2\tau - 1). \tag{B25}$$

Differentiating Eq. (B24) with respect to x_j yields

$$\frac{\partial \Pi_{ij}^{(1)}}{\partial x_j} = \nu\frac{\partial}{\partial x_j}\left[\frac{\partial (\rho u_i)}{\partial x_j} + \frac{\partial (\rho u_j)}{\partial x_i} + \frac{\partial (\rho u_k)}{\partial x_k}\delta_{ij}\right]. \tag{B26}$$

After applying the continuity Eq. (20) to the above, we have

$$\frac{\partial \Pi_{ij}^{(1)}}{\partial x_j} = \nu\frac{\partial^2 (\rho u_i)}{\partial x_j^2}. \tag{B27}$$

Combining this with Eq. (B18) results in

$$\frac{\partial (\rho u_i)}{\partial t} + \frac{\partial (\rho u_i u_j)}{\partial x_j} = F_i - \frac{\partial p}{\partial x_i} + \nu\frac{\partial^2 (\rho u_i)}{\partial x_j^2}. \tag{B28}$$

Again, the density variation is assumed to be small enough, the above is just the Navier-Stokes Eq. (21) for incompressible flows.

[1] S. Chen and G. D. Doolen, Annu. Rev. Fluid Mech. **30**, 329 (1998).

[2] K. Sankaranarayanan, X. Shan, I. G. Kevrekidis, and S. Sundaresan, Chem. Eng. Sci. **54**, 4817 (1999).

[3] S. Succi, *The Lattice Boltzmann Equation for Fluid Dynamics and Beyond* (Oxford, London, 2001).

[4] D. Yu, R. Mei, and W. Shyy, Int. J. Numer. Methods Fluids **39**, 99 (2002).

[5] J. G. Zhou, *Lattice Boltzmann Methods for Shallow Water Flows* (Springer-Verlag, Berlin, 2004).

[6] M. C. Sukop and D. T. J. Thorne, *Lattice Boltzmann Modeling: An Introduction for Geoscientists and Engineers* (Springer-

Verlag, Berlin, 2006).
[7] J. G. Zhou, Int. J. Mod. Phys. C **18**, 973 (2007).
[8] Y. T. Chew, C. Shu, and X. D. Niu, J. Stat. Phys. **107**, 329 (2002).
[9] R. W. Mei and W. Shyy, J. Comput. Phys. **143**, 426 (1998).
[10] M. Stiebler, J. Tölke, and M. Krafczyk, Comput. Fluids **35**, 814 (2006).
[11] O. Filippova and D. Hänel, J. Comput. Phys. **147**, 219 (1998).
[12] X. He, L.-S. Luo, and M. Dembo, J. Comput. Phys. **129**, 357 (1996).
[13] H. R. Wu, Y. L. He, G. H. Tang, and W. Q. Tao, Prog. Comput. Fluid Dyn. **5**, 97 (2005).
[14] B. Mondal and S. C. Mishra, Int. J. Heat Mass Transfer **51**, 68 (2008).
[15] S. C. Mishra, B. Mondal, T. Kush, and B. S. R. Krishna, Int. Commun. Heat Mass Transf. **36**, 322 (2009).
[16] P. Lallemand and L.-S. Luo, Phys. Rev. E **61**, 6546 (2000).
[17] M. Bouzidi, D. d'Humières, P. Lallemand, and L.-S. Luo, J. Comput. Phys. **172**, 704 (2001).
[18] P. L. Bhatnagar, E. P. Gross, and M. Krook, Phys. Rev. **94**, 511 (1954).
[19] Y. Peng, C. Shu, Y. Chew, and J. Qiu, J. Comput. Phys. **186**, 295 (2003).
[20] X. D. Niu, C. Shu, and Y. T. Chew, Int. J. Mod. Phys. C **14**, 785 (2003).
[21] K. N. Premnath and J. Abraham, Phys. Rev. E **71**, 056706 (2005).
[22] T. Reis and T. N. Phillips, Phys. Rev. E **75**, 056703 (2007).
[23] S. Mukherjee and J. Abraham, Phys. Rev. E **75**, 026701 (2007).
[24] I. Halliday, L. A. Hammond, C. M. Care, K. Good, and A. Stevens, Phys. Rev. E **64**, 011208 (2001).
[25] J. G. Zhou, Phys. Rev. E **78**, 036701 (2008).
[26] Z. Guo, H. Han, B. Shi, and C. Zheng, Phys. Rev. E **79**, 046708 (2009).
[27] J. G. Zhou, Int. J. Mod. Phys. C **12**, 387 (2001).
[28] R. J. LeVeque, J. Comput. Phys. **146**, 346 (1998).
[29] A. Bermudez and M. E. Vázquez, Comput. Fluids **23**, 1049 (1994).
[30] I. L. Rozovskii, *Flow of Water in Bends of Open Channels* (Israel Program for Scientific Translation, Jerusalem, 1965).
[31] J. G. Zhou, Comput. Methods Appl. Mech. Eng. **191**, 3527 (2002).
[32] P. Drazin and N. Riley, *The Navier-Stokes Equations: A Classification of Flows and Exact Solutions*, Lecture Notes Series 334 (Cambridge University Press, England, 2006).
[33] Q. Zou and X. He, Phys. Fluids **9**, 1591 (1997).